DIST LOSS: ENHANCING REGRESSION IN FEW-SHOT REGION THROUGH DISTRIBUTION DISTANCE CONSTRAINT

Anonymous authors
Paper under double-blind review

ABSTRACT

Imbalanced data distributions are prevalent in real-world scenarios, posing significant challenges in both imbalanced classification and imbalanced regression tasks. They often cause deep learning models to overfit in areas of high sample density (many-shot regions) while underperforming in areas of low sample density (few-shot regions). This characteristic restricts the utility of deep learning models in various sectors, notably healthcare, where areas with few-shot data hold greater clinical relevance. While recent studies have shown the benefits of incorporating distribution information in imbalanced classification tasks, such strategies are rarely explored in imbalanced regression. In this paper, we address this issue by introducing a novel loss function, termed Dist Loss, designed to minimize the distribution distance between the model's predictions and the target labels in a differentiable manner, effectively integrating distribution information into model training. Dist Loss enables deep learning models to regularize their output distribution during training, effectively enhancing their focus on few-shot regions. We have conducted extensive experiments across three datasets spanning computer vision and healthcare: IMDB-WIKI-DIR, AgeDB-DIR, and ECG-Ka-DIR. The results demonstrate that Dist Loss effectively mitigates the negative impact of imbalanced data distribution on model performance, achieving state-of-the-art results in sparse data regions. Furthermore, Dist Loss is easy to integrate, complementing existing methods. Our code will be made publicly available following the review process.

1 INTRODUCTION

Imbalanced data distributions are prevalent in the real world, with certain target values being significantly underrepresented Buda et al. (2018); Liu et al. (2019). In regression tasks, conventional deep learning models tend to predict towards regions of high sample density (many-shot regions) during training to minimize overall error. This results in models that perform well on the majority of samples but exhibit significantly higher prediction errors on regions of low sample density (few-shot regions). This phenomenon severely limits the applicability of deep learning models in certain contexts, such as healthcare scenarios where minority samples often carry significant importance, and significant errors in these samples could lead to potential adverse events.

Taking the prediction of potassium concentration based on electrocardiogram (ECG) as an example, the model takes ECG signals as input and outputs the predicted potassium concentration derived from ECG signal features. Figure 1a illustrates the distribution of potassium concentrations in a real-world dataset, where the majority of samples fall within the normal range, and the minority of abnormal potassium concentrations (potassium concentration $\leq$ 3.5 mmol/L or $\geq$ 5.5 mmol/L) are mostly found in the few-shot region. Due to the imbalanced data distribution, traditional deep learning models tend to predict abnormal potassium concentration samples as normal to minimize overall error. However, since abnormal potassium concentrations significantly affect metabolism and cardiac function, they can lead to serious consequences such as arrhythmias or sudden death Ferreira et al. (2020); Crotti et al. (2020); Kim et al. (2023). Therefore, in clinical settings, the focus is often on accurately predicting the minority of abnormal potassium concentrations Galloway et al. (2019); Harmon et al. (2024), which is challenging for traditional deep learning models. Hence,

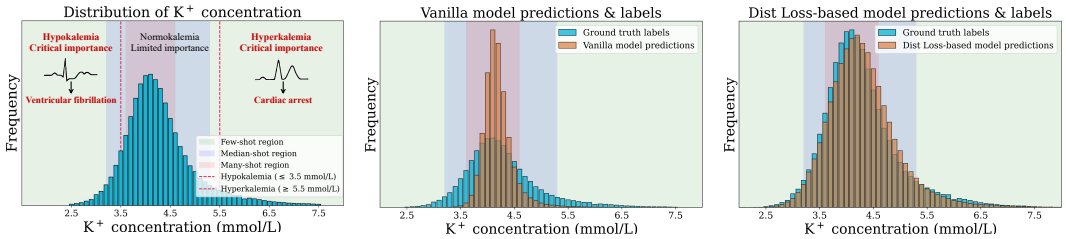

(a) (b) (c)

Figure 1: A real-world healthcare task of potassium (K^+) concentration regression from ECGs. (a) Both hyperkalemia (high K^+) and hypokalemia (low K^+) are predominantly found in the few-shot region, with normal K^+ are located in the many-shot region. Hyperkalemia and hypokalemia are life-threatening conditions that can lead to cardiac arrest and ventricular fibrillation, necessitating accurate and timely detection. Conversely, normal K^+ concentrations (the many-shot region) are of little concern, as inaccurate and untimely detection of these samples has minimal impact. Here, we follow Yang et al. (2021) to define the few-, median-, many-shot regions. (b) illustrates the significant distribution discrepancy between the vanilla model's predictions and the labels, stemming from the imbalanced data distribution. Here, the term "vanilla model" refers to a model that employs no specialized techniques to address imbalanced data. The orange histogram represents the label distribution, while the blue histogram depicts the prediction distribution from the vanilla model. It is evident that the model's predictions are heavily concentrated in the many-shot region and seldom fall into the few-shot region. (c) demonstrates the effectiveness of Dist Loss in reducing the distribution discrepancy. The orange histogram indicates the label distribution, and the blue histogram shows the prediction distribution from the model enhanced with Dist Loss. It is clear that the distribution discrepancy is significantly reduced.

how to effectively enhance model accuracy in few-shot regions under imbalanced data distributions is of significant importance and value.

In imbalanced regression tasks, a significant issue is the substantial discrepancy between the model's prediction distribution and the label distribution, as demonstrated in Figure 1b. The orange histogram in the figure represents the ground truth, whereas the blue histogram shows the distribution of the model's predictions. It is evident that the model's predictions are primarily concentrated in the many-shot region, while very few predictions occur in the few-shot region. This observation highlights a critical consequence of imbalanced data distributions: the marked deviation between the model's prediction distribution and the true label distribution. While prior research has mitigated the adverse effects on minority classes in imbalanced classification by integrating distribution information into the training process Feng et al. (2018); Zheng et al. (2020); Tian et al. (2020), such strategies are rarely explored in the context of imbalanced regression. **Thus, it is crucial to explore whether significant prediction errors in few-shot regions, resulting from imbalanced data distributions, can be effectively mitigated by utilizing distribution information to align the prediction distribution of the model with the label distribution.**

Based on this concept, we introduce a novel loss function named Dist Loss, which aims to minimize the distance between model's prediction distribution and the label distribution. Dist Loss is implemented in three key steps: (1) Generating pseudo-labels: we use kernel density estimation (KDE) Parzen (1962) to model the probability distribution of labels and generate pseudo-labels from this distribution; (2) Creating pseudo-predictions: we sort the model's predictions to create pseudo-predictions that reflect the prediction distribution; (3) Distance approximation: we approximate the distance between the prediction and label distributions by measuring the distance between the pseudo-labels and pseudo-predictions. By optimizing both the distribution distance and sample-level prediction errors during training, Dist Loss reduces errors in individual predictions and aligns the model's predictions with the label distribution. This approach effectively solves the distribution discrepancy introduced by imbalanced data distributions, as shown in 1c, thus improving the accuracy in predicting few-shot regions.

To validate the effectiveness of Dist Loss, we have conducted comprehensive experiments on three datasets across computer vision and healthcare: IMDB-WIKI-DIR, AgeDB-DIR, and our meticu-

lously crafted ECG-Ka-DIR dataset. The findings indicate that our approach achieves a substantial increase in accuracy for rare samples, thereby attaining state-of-the-art (SOTA) performance. Moreover, our experiments reveal that Dist Loss can be integrated with existing techniques, culminating in further enhanced outcomes.

In summary, the contributions of this paper are:

- We reexamine the impact of imbalanced data distributions in regression tasks from the perspective of distribution discrepancy and introduce the concept of aligning a model's prediction distribution with the label distribution by leveraging distribution priors.
- We propose a novel, differentiable approach for measuring the distribution distance in regression tasks, extending distribution distance optimization techniques from classification tasks to regression domains.
- Through extensive experiments on multiple datasets, we validate the effectiveness of Dist Loss in deep imbalanced regression, achieving SOTA performance in few-shot regions.

2 Related work

2.1 Imbalanced classification

Research on the problem of imbalanced classification mainly focuses on improving the loss function to enhance the model's ability to identify the minority class. Weighted cross entropy King & Zeng (2001) gives higher weights to minority class samples, allowing the model to pay more attention to minority class samples when facing class imbalance. Focal loss Lin (2017) reduces the influence of the majority class by dynamically adjusting the weights in the loss function, further improving the performance of the minority class. Combining data augmentation and resampling techniques is also a common strategy. RUSBoost Seiffert et al. (2009) combines random undersampling and boosting to reduce the majority class while maintaining the performance of the model. SMOTE Chawla et al. (2002) further improves the classification results by expanding the minority class data through synthetic samples. The combination of adversarial training and loss functions has also gradually attracted attention, and adversarial reweighting Sagawa et al. (2019) improves the accuracy of minority classes.

2.2 Imbalanced regression

Unlike imbalanced classification, regression tasks can have labels that are infinite and boundless, which prevents methods designed for imbalanced classification from being directly transferred to imbalanced regression. Consequently, existing methods focus on leveraging the continuity of the label space. At the input level, methods addressing imbalanced regression primarily focus on resampling the training dataset. SMOTE Chawla et al. (2002); Torgo et al. (2013) and its variant SMOGN Branco et al. (2017) generate new samples by leveraging the differences between minority samples and their nearest neighbors. Branco et al. (2018) integrates a bagging-based ensemble method with SMOTE to mitigate the impact of imbalanced data distributions on the model. At the feature level, Yang et al. (2021) proposes feature distribution smoothing (FDS) by transferring feature statistics between nearby target bins to smooth the feature space. VIR Wang & Wang (2024) borrows data with similar regression labels to compute the variational distribution of the latent representation. Ranksim Gong et al. (2022) uses contrastive learning to bring the feature space of samples with similar labels closer and push the feature space of samples with dissimilar labels apart. ConR Keramati et al. (2024) designs positive and negative sample pairs based on label similarity, transferring the label space relationships to the feature space in a contrastive manner, too. At the model output and label level, regressor retraining (RRT) Yang et al. (2021) decouples the training of the encoder and regressor, retraining the regressor with inverse reweighting after normal encoder training. DenseLoss Steininger et al. (2021) and label distribution smoothing (LDS) Yang et al. (2021) measure label rarity through KDE and assign weights to each sample, with rare samples being assigned higher weights to enhance the model's focus on minority samples. Balanced MSE Ren et al. (2022) leverages the training label distribution prior to restore a balanced prediction.

However, existing research on deep imbalanced regression often overlooks the significant distribution discrepancy between model's predictions and labels, and distribution information, which has

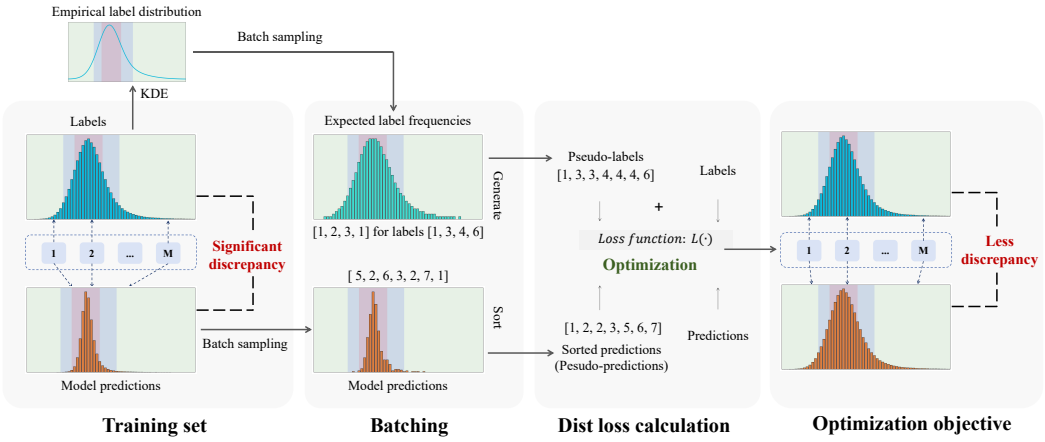

Figure 2: The presence of imbalanced data distributions introduces a noticeable discrepancy between the model's prediction and label distributions. Dist Loss mitigates the impact of this imbalance by minimizing this discrepancy. Initially, KDE is utilized to ascertain the distribution of labels and to calculate the expected frequencies of each label within a batch, thereby generating pseudo-labels imbued with the label distribution information. For example, given the labels [1, 3, 4, 6] and their calculated expected frequencies [1, 2, 3, 1], the resulting pseudo-labels would be [1, 3, 3, 4, 4, 4, 6], where each label is repeated according to its calculated frequency. Subsequently, the model's predictions within a batch are sorted to yield an ordered sequence of predictive values. Assuming the model's initial predictions are [5, 2, 6, 3, 2, 7, 1], the sorted sequence, which encapsulates the prediction distribution information, would be [1, 2, 2, 3, 5, 6, 7]. Measuring the distance between these pseudo-labels and pseudo-predictions, both equipped with respective distribution information, provides an approximation of the distribution distance. Thereafter, by simultaneously optimizing the distribution distance and sample-level prediction errors during the training process, the model can effectively alleviate the negative effects of imbalanced data, significantly enhancing its accuracy in few-shot regions.

been proven effective in imbalanced classification, is rarely utilized. In contrast, our approach focuses on concurrently aligning the prediction distribution with the label distribution and reducing sample-level prediction errors during the training process. This significantly improves the model's accuracy on few-shot regions without incurring additional computational costs or requiring meticulous hyperparameter tuning. Extensive experiments demonstrate the superiority of our approach in handling critical and informative rare samples in few-shot regions, achieving SOTA results.

3 METHOD

3.1 PROBLEM SETTING

Let $\mathcal{D}$ be a training dataset comprising N samples, denoted as $\mathcal{D} = \{(\mathbf{x}_{(i)}, y_{(i)})\}_{i=1}^{N}$, where $\mathbf{x}_{(i)} \in \mathbb{R}^d$ represents the input and $y_{(i)} \in \mathbb{R}$ denotes the corresponding label. To facilitate processing, the continuous label space $\mathcal{Y}$ is discretized into B bins of equal width: $\mathcal{Y} = \bigcup_{b=1}^{B} [y_b, y_{b+1})$, where y_b is the lower bound of bin b, and $y_1 < y_2 < \cdots < y_B$. In subsequent discussions, for convenience, the lower bound y_b of the bin $[y_b, y_{b+1})$ will represent any label value $y_{(i)}$ that falls within that bin. Similarly, the model prediction space $\hat{\mathcal{Y}}$ is partitioned into bins of equal width. In practical scenarios, the width of each bin, denoted Δ_y, indicates the minimum resolution of interest when processing the label space. For instance, in age estimation, one might set the bin width to 1, resulting in: $\Delta_y = y_{b+1} - y_b = 1, \quad \forall b \in \mathcal{B}$. Additionally, we define the probability of observing a label y_i as p_i, and the probability distribution of labels can be estimated using KDE.

3.2 DIST LOSS

One of the optimization objectives of Dist Loss is to minimize the distance between the prediction and label distributions in regression tasks. The core challenge lies in measuring the distance between these two distributions in a differentiable manner. Traditional metrics for measuring distribution distance, such as Kullback-Leibler divergence and Jensen-Shannon divergence, cannot be implemented in a differentiable form for regression tasks. Therefore, we have devised an alternative approach in the implementation of Dist Loss to realize a differentiable distribution distance measurement in regression scenarios. Specifically, we approximate the distance between the label and prediction distributions by sampling from these distributions and quantifying the differences between the sampled values to estimate the distance.

3.2.1 CALCULATION OF DIST LOSS

As illustrated in Figure 2, we sample from the label and prediction distributions to generate pseudo-labels and pseudo-predictions, which encapsulate the distribution information of the labels and predictions. Taking the generation of pseudo-labels as an example, we will now detail the process.

To generate pseudo-labels that contain label distribution information, we first randomly sample M points from the label distribution. The expected frequencies of the label y_i can be estimated by multiplying the number of sampling points M by the probability of that label p_i. Based on this, we construct a sequence $\mathcal{N}_L = (n_1, n_2, \cdots, n_B)$ to represent these expected frequencies, where $n_i = M \cdot p_i$. Each element in the obtained $\mathcal{N}_L$ represents the expected frequencies of the corresponding label. Since these frequencies may be fractional, we need to convert them to integers while ensuring that the sum after conversion still equals M. Here, we denote the converted integer sequence by $\mathcal{N}_{L'} = (n'_1, n'_2, \cdots, n'_B)$. To acquire $\mathcal{N}_{L'}$, we first take the floor of each element in $\mathcal{N}_L$ to obtain the sequence $\mathcal{N}_{L_f} = (\lfloor n_1 \rfloor, \lfloor n_2 \rfloor, \cdots, \lfloor n_B \rfloor)$. Then we calculate the difference a, which represents the difference between the sum of the original expected frequencies (M) and the sum after applying the floor function, following $a = M - \sum_{i=1}^{B} \lfloor n_i \rfloor$. Using the difference a, we construct an auxiliary sequence $\mathcal{A}$, which determines how to evenly distribute the difference to the elements of $\mathcal{N}_{L_f}$ to ensure the sum is M:

$$a_i = \begin{cases} 1, & \text{if } i \leq \left\lfloor \frac{a+1}{2} \right\rfloor \text{ or } i > B - \left\lfloor \frac{a}{2} \right\rfloor \\ 0, & \text{otherwise} \end{cases}, \tag{1}$$

Each n'_i is determined by adding a_i to the corresponding element in $\mathcal{N}_{L_f}$, where $n'_i = \lfloor n_i \rfloor + a_i$, and i $\in \mathcal{B}$. Finally, we generate the corresponding pseudo-labels $\mathcal{S}_L$ based on the expected frequencies, where each element S_{L_j} is represented as:

$$S_{L_j} = \min_{i \in \mathcal{B}} \left(y_i \cdot \theta \left(\sum_{k=1}^{i} n'_k - j \right) \right), \tag{2}$$

Here, $\theta(x)$ is the unit step function, which returns 1 when $x \geq 0$ and 0 otherwise. To illustrate with a specific example, assume that the label sequence is $(y_1, y_2, y_3) = (4, 5, 6)$ and that the obtained sequence $\mathcal{N}_{L'}$ is $(1, 2, 3)$. Then, the generated pseudo-labels S_L would be $(4, 5, 5, 6, 6, 6)$.

Similarly, we can perform M-point sampling on the prediction distribution and subsequently apply the same operations to obtain the pseudo-predictions $\mathcal{S}_P$, which encapsulate information about the prediction distribution.

In practice, we can consider a batch during the model training process as a random sampling event, wherein the model predictions within a batch are viewed as the sampling values of the prediction distribution. Consequently, we do not need to repeat the aforementioned process to acquire pseudo-predictions; instead, we simply sort the model predictions in the batch, which already contains the prediction information. By measuring the distance between the pseudo-predictions and the pseudo-labels, we can approximate the distance between the respective distributions. Let us denote the function $L(\cdot)$ as a measure of the distance between two sequences; then, the distribution distance can be expressed as $L(\mathcal{S}_P, \mathcal{S}_L)$. Furthermore, using the function $L(\cdot)$, we can simultaneously assess the sample-level prediction errors, which reflect the difference between the predicted values and the

labels. Ultimately, by synchronously optimizing both the distribution distance and the sample-level prediction errors during the training process, we can mitigate the issue of distribution discrepancy, thereby addressing the challenges posed by imbalanced data distributions.

3.2.2 Fast Differentiable Sorting

As previously mentioned, the obtained pseudo-predictions are in ascending order, whereas the order of the model's actual predictions is random in practical scenarios. Therefore, it is necessary to sort the model's predictions to obtain the pseudo-predictions. Since the sorting operation is non-differentiable, we employ a fast differentiable sorting algorithm Blondel et al. (2020) to ensure the differentiability of the entire computation process.

This method achieves the sorting operation by defining it as projections on permutation polytopes. Specifically, for any given vector $w \in \mathbb{R}^n$, we construct the permutation polytope $P(w)$, which represents the convex hull of all possible permutations of w, i.e.,

$$P(w) := \text{conv}(\{w_\sigma : \sigma \in \Sigma\}), \tag{3}$$

where Σ denotes all permutations of $[n]$. The sorting operation $s(\theta)$ is defined as the solution to the linear programming problem that maximizes the dot product with ρ (a strictly decreasing vector) on $P(\theta)$, i.e.,

$$s(\theta) = \arg\max_{y \in P(\theta)} \langle y, \rho \rangle. \tag{4}$$

To ensure the differentiability of the sorting operation, a regularization term Ψ is introduced, transforming the sorting operation into tractable projection problems:

$$P_\Psi(z, w) = \arg\min_{\mu \in P(w)} \left\{ \frac{1}{2}\|\mu - z\|^2 + \Psi(\mu) \right\}, \tag{5}$$

where Ψ is a strongly convex function, ensuring the differentiability of the problem. This approach enables forward propagation with $O(n \log n)$ time complexity and backward propagation with $O(n)$ time complexity.

4 Experiments

4.1 Benchmarks and baselines

We evaluated our method on three datasets, focusing on tasks of age estimation and potassium concentration prediction. The IMDI-WIKI-DIR dataset Yang et al. (2021), derived from the IMDB-WIKI dataset Rothe et al. (2018), consists of 213,553 facial image pairs annotated with age information. This dataset is partitioned into 191,509 samples for training, 11,022 for validation, and 11,022 for testing. The AgeDB-DIR dataset Yang et al. (2021), derived from the AgeDB dataset Moschoglou et al. (2017), comprises 16,488 facial image pairs with age annotations. It is divided into 12,208 samples for training, 2,140 for validation, and 2,140 for testing. The ECG-Ka-DIR dataset, sourced from the MIMIC-IV dataset Johnson et al. (2020), includes 375,745 pairs of single-lead ECG signals paired with potassium concentration values. This dataset is divided into 365,549 samples for training, 5,098 for validation, and 5,098 for testing. All these datasets are characterized by imbalanced training sets and balanced validation and test sets. The label distributions of these three datasets are shown in Figure 3. Please refer to Appendix A.1 and A.2 for baseline and implementation details.

4.2 Evaluation metrics

Following the evaluation metrics of Yang et al. (2021), we report the results for four shots: all, many, median, and few, where all represents the entire dataset, and many/median/few correspond to areas of high/medium/low sample density within the dataset. For the IMDB-WIKI-IR and AgeDB-DIR datasets, we maintain consistency with previous studies, where few/median/many correspond to areas with fewer than 20, between 20-100, and more than 100 samples, respectively. For the ECG-Ka-DIR dataset, assuming that the maximum number of samples for a single label is n_{max},

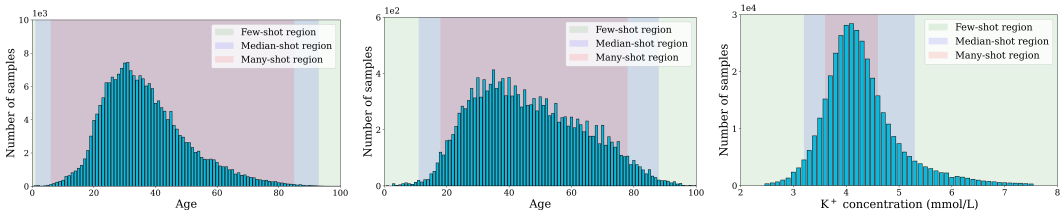

(a) IMDB-WIKI-DIR (b) AgeDB-DIR (c) ECG-Ka-DIR

Figure 3: Overview of label distributions in the training sets for the IMDB-WIKI-DIR, AgeDB-DIR, and ECG-Ka-DIR datasets. The classification of shot types for IMDB-WIKI-DIR and AgeDB-DIR follows the definitions provided in Yang et al. (2021).

we define areas with more than 0.5 n_{max}, between 0.15-0.5 n_{max}, and fewer than 0.15 n_{max} samples as many/median/few shots areas, respectively. For each dataset, we report the mean absolute error (MAE) and the geometric mean (GM).

4.3 Main Results

Table 1 presents the results of baselines and our method in the few-shot region across three datasets, along with a comparison of these results. For detailed results on each dataset, please refer to Appendix A.3. This table is divided into two sections. The first section displays the results of the baselines and our method, with the best results highlighted in bold and red. The second section shows the improvement of our method over each baseline, with green bold indicating superior performance of our method and blue bold indicating otherwise. From the first section of the table, it is evident that our method achieves the best results in five out of six metrics across the three datasets, with SOTA performances of 22.550, 9.122, and 1.329 on the IMDB-WIKI-DIR, AgeDB-DIR, and ECG-Ka-DIR datasets, respectively. The second section reveals that our method outperforms in 28 out of 30 metrics. Notably, compared to Balanced MSE, which also involves fine-tuning the linear layers of a pre-trained model and employs data distribution priors, our method demonstrates superior performance in the few-shot region, highlighting the effectiveness of our approach.

Table 2 further illustrates the complementary nature of our method with existing approaches. This table is divided into five sections, each showcasing the results of one baseline and the combined results with our method, with the best results within each section highlighted in bold and black. From this table, it is shown that our method achieves better results in 26 out of 30 metrics. Taking the MAE metric as an example, incorporating our method leads to improved performance in the few-shot region across all three datasets, achieving the best results of 22.331, 9.110, and 1.325 on the IMDB-WIKI-DIR, AgeDB-DIR, and ECG-Ka-DIR datasets, respectively. These experimental results demonstrate a key advantage of our method, namely its ability to effectively complement existing methods, thereby enhancing model performance in the few-shot region.

4.4 Time Consumption Analysis

Table 3 presents the time required to train each method for one epoch on the IMDB-WIKI-DIR, AgeDB-DIR, and ECG-Ka-DIR datasets, with all times reported in seconds. It can be observed that Balanced MSE and Dist Loss have the shortest training times, attributed to their approach of fine-tuning the model's linear layers. The time consumption of LDS and the vanilla model are largely consistent, as these methods only weight the loss function without significantly increasing computational load. For methods operating at the feature level, including FDS, Ranksim, and ConR, a notable increase in model training time is evident, due to the computational intensity associated with feature-level operations.

Table 1: Results are presented for the few-shot region on the IMDB-WIKI-DIR, AgeDB-DIR, and ECG-Ka-DIR datasets. The first section of the table reports the results of baselines and our method, with the best results highlighted in bold and red. In the second section, improvements over corresponding baselines are reported in bold and green, while decreases in performance are reported in bold and blue.

	MAE			GM		
	IMDB-WIKI-DIR	AgeDB-DIR	ECG-Ka-DIR	IMDB-WIKI-DIR	AgeDB-DIR	ECG-Ka-DIR
Vanilla	26.930	12.894	1.771	21.254	9.789	1.578
+ LDS	22.753	11.279	1.510	12.803	7.846	1.190
+ FDS	24.908	11.161	1.737	14.361	7.361	1.529
+ Ranksim	25.999	12.569	1.791	19.690	9.495	1.600
+ ConR	25.408	12.623	1.756	17.022	8.787	1.556
+ Balanced MSE	23.542	9.613	1.417	**12.603**	6.248	1.046
+ **Dist Loss (Ours)**	**22.550**	**9.122**	**1.329**	14.288	**5.453**	**0.978**
Ours vs. Vanilla	**+ 4.380**	**+ 3.772**	**+ 0.442**	**+ 6.966**	**+ 4.336**	**+ 0.600**
Ours vs. LDS	**+ 0.203**	**+ 2.157**	**+ 0.181**	**- 1.485**	**+ 2.393**	**+ 0.212**
Ours vs. FDS	**+ 2.358**	**+ 2.039**	**+ 0.408**	**+ 0.073**	**+ 1.908**	**+ 0.551**
Ours vs. Ranksim	**+ 3.449**	**+ 3.447**	**+ 0.462**	**+ 5.402**	**+ 4.042**	**+ 0.622**
Ours vs. ConR	**+ 2.858**	**+ 3.501**	**+ 0.427**	**+ 2.734**	**+ 3.334**	**+ 0.578**
Ours vs. Balanced MSE	**+ 0.992**	**+ 0.491**	**+ 0.088**	**- 1.685**	**+ 0.795**	**+ 0.068**

Table 2: Results are presented for the few-shot region on the IMDB-WIKI-DIR, AgeDB-DIR, and ECG-Ka-DIR datasets. Each section of the table reports the results of a baseline and the baseline incorporating our method, with the better results highlighted in bold.

	MAE			GM		
	IMDB-WIKI-DIR	AgeDB-DIR	ECG-Ka-DIR	IMDB-WIKI-DIR	AgeDB-DIR	ECG-Ka-DIR
+ LDS	22.753	11.279	1.510	**12.803**	7.846	1.190
+ LDS + **Dist Loss**	**22.331**	**10.437**	**1.325**	13.021	**7.051**	**0.957**
+ FDS	24.908	11.161	1.737	**14.361**	7.361	1.529
+ FDS + **Dist Loss**	**24.112**	**10.444**	**1.428**	14.929	**6.696**	**1.099**
+ Ranksim	25.999	12.569	1.791	19.690	9.495	1.600
+ Ranksim + **Dist Loss**	**23.772**	**12.102**	**1.325**	**15.422**	**8.515**	**0.970**
+ ConR	25.408	12.623	1.756	17.022	**8.787**	1.556
+ ConR + **Dist Loss**	**22.700**	**12.303**	**1.336**	**14.713**	9.123	**0.987**
+ Balanced MSE	23.542	9.613	1.417	**12.603**	6.248	1.046
+ Balanced MSE + **Dist Loss**	**22.597**	**9.110**	**1.357**	14.238	**5.585**	**0.996**

Table 3: Time consumption (in seconds) of one training epoch for the IMDB-WIKI-DIR, AgeDB-DIR, and ECG-Ka-DIR datasets, with batch sizes of 64, 64, and 256, respectively.

	IMDB-WIKI-DIR	AgeDB-DIR	ECG-Ka-DIR
Vanilla	399.8	31.8	94.6
+ LDS	401.2	31.4	104.0
+ FDS	567.5	43.6	155.1
+ Ranksim	512.6	40.2	135.1
+ ConR	1168.7	91.6	192.1
+ Balanced MSE	152.6	14.2	51.8
+ **Dist Loss (Ours)**	154.0	15.1	58.7

Table 4: Ablation study on loss functions measuring sequence difference. L_1 represents MAE Loss, L_2 represents MSE Loss, $INV-$ denotes the probability-based inversely weighted version of these loss functions. Results on the few-shot region are reported, with the best results in each section are in bold.

	MAE			GM		
	IMDB-WIKI-DIR	AgeDB-DIR	ECG-Ka-DIR	IMDB-WIKI-DIR	AgeDB-DIR	ECG-Ka-DIR
Vanilla	26.930	12.894	1.771	21.254	9.789	1.578
+ Dist Loss ($INV-L_1$)	23.334	9.802	1.467	15.437	6.298	1.044
+ Dist Loss ($INV-L_2$)	**22.516**	**9.122**	**1.329**	**13.752**	**5.453**	**0.978**
+ LDS	22.753	11.279	1.510	12.803	7.846	1.190
+ Dist Loss ($INV-L_1$)	**22.178**	**9.872**	1.413	**11.334**	**6.109**	0.984
+ Dist Loss ($INV-L_2$)	22.331	10.437	**1.325**	13.021	7.051	**0.957**
+ FDS	24.908	11.161	1.737	**14.361**	7.361	1.529
+ Dist Loss ($INV-L_1$)	**23.692**	**9.969**	1.515	14.399	**6.026**	1.122
+ Dist Loss ($INV-L_2$)	24.112	10.444	**1.428**	14.929	6.696	**1.099**
+ Ranksim	25.999	12.569	1.791	19.690	9.495	1.600
+ Dist Loss ($INV-L_1$)	23.894	**11.877**	1.577	16.036	**8.164**	1.330
+ Dist Loss ($INV-L_2$)	**23.772**	12.102	**1.325**	**15.422**	8.515	**0.970**
+ ConR	25.408	12.623	1.756	17.022	8.787	1.556
+ Dist Loss ($INV-L_1$)	23.281	**11.948**	1.452	15.586	**8.605**	1.044
+ Dist Loss ($INV-L_2$)	**22.700**	12.303	**1.336**	**14.713**	9.123	**0.987**
+ Balanced MSE	23.542	9.613	1.417	**12.603**	6.248	1.046
+ Dist Loss ($INV-L_1$)	23.539	9.762	1.474	15.000	6.198	1.051
+ Dist Loss ($INV-L_2$)	**22.597**	**9.110**	**1.357**	14.238	**5.585**	**0.996**

4.5 Ablations and analysis

4.5.1 Different loss functions for sequence difference measurement

Dist Loss employs the loss function $L(\cdot)$ to measure the difference between two sequences. In this ablation study, we demonstrate the effects of using different functions, considering the probability-based inversely weighted MAE and MSE losses. The experimental results are shown in Table 4, where detailed results on each dataset are shown in Appendix A.4.2. The table illustrates that Dist Loss reliably boosts model accuracy in the few-shot region.

4.5.2 Different batch sizes for distribution distance approximation

Dist Loss estimates the overall distribution distance between predictions and labels by measuring batch-wise distances during training. This ablation study evaluates the sensitivity of model accuracy to batch size, as detailed in Table 5. We examined batch sizes of 256, 512, and 768, adopting 256 as a standard based on prior research Yang et al. (2021); Gong et al. (2022). The findings show negligible variations in performance with different batch sizes. This could be attributed to the fact that accurate distribution information is more critical during sampling than the precise accuracy of individual pseudo-labels.

4.5.3 Dist Loss Surpasses Existing Methods in the Median-Shot Region

As depicted in the supplementary Tables 6, 7, and 8 within Appendix A.3, Dist Loss delivers SOTA results, excelling not only in few-shot regions but also in median-shot regions. In our comparison with current methods, Dist Loss achieved the lowest MAE and the second-lowest GM on the IMDB-WIKI-DIR and AgeDB-DIR datasets, with scores of 12.614/7.686 and 7.315/4.563, respectively. Similarly, on the ECG-Ka-DIR dataset, it secured the highest GM and the second-lowest MAE, recording 0.445 and 0.674, respectively. Moreover, our experiments show that integrating Dist Loss with existing methods consistently improved performance in median-shot regions when measured by both MAE and GM, surpassing the results of using those methods alone on IMDB-WIKI-DIR and AgeDB-DIR datasets. On the ECG-Ka-DIR dataset, this integration notably increased the GM. In conclusion, these findings validate Dist Loss's efficacy in enhancing model accuracy in both few-shot and median-shot regions.

Table 5: Ablation study on batch sizes for Dist Loss. Results on the few-shot region are reported.

	MAE		GM	
	IMDB-WIKI-DIR		AgeDB-DIR	
256	22.323	9.013	13.787	5.632
512	22.516	9.122	13.752	5.453
768	22.550	9.148	14.288	5.223

5 CONCLUSION

In this study, we address the significant escalation of prediction errors in few-shot regions, a prevalent challenge in deep imbalanced regression. By leveraging distribution priors, we introduce a novel loss function, Dist Loss, designed to align the model's prediction distribution with the label distribution throughout the training process. Our extensive experimental evaluation demonstrates that Dist Loss effectively enhances prediction accuracy in few-shot regions, achieving state-of-the-art performance. Furthermore, our results indicate that Dist Loss can be seamlessly integrated with existing methods to further augment their efficacy. We hope our work underscores the critical role of integrating distribution information in tackling deep imbalanced regression tasks.

REFERENCES

Mathieu Blondel, Olivier Teboul, Quentin Berthet, and Josip Djolonga. Fast differentiable sorting and ranking. In *International Conference on Machine Learning*, pp. 950–959. PMLR, 2020.

Paula Branco, Luís Torgo, and Rita P Ribeiro. Smogn: a pre-processing approach for imbalanced regression. In *First international workshop on learning with imbalanced domains: Theory and applications*, pp. 36–50. PMLR, 2017.

Paula Branco, Luis Torgo, and Rita P. Ribeiro. Rebagg: Resampled bagging for imbalanced regression. In Luís Torgo, Stan Matwin, Nathalie Japkowicz, Bartosz Krawczyk, Nuno Moniz, and Paula Branco (eds.), *Proceedings of the Second International Workshop on Learning with Imbalanced Domains: Theory and Applications*, volume 94 of *Proceedings of Machine Learning Research*, pp. 67–81. PMLR, 10 Sep 2018.

Mateusz Buda, Atsuto Maki, and Maciej A Mazurowski. A systematic study of the class imbalance problem in convolutional neural networks. *Neural networks*, 106:249–259, 2018.

Nitesh V Chawla, Kevin W Bowyer, Lawrence O Hall, and W Philip Kegelmeyer. Smote: synthetic minority over-sampling technique. *Journal of artificial intelligence research*, 16:321–357, 2002.

Lia Crotti, Katja E Odening, and Michael C Sanguinetti. Heritable arrhythmias associated with abnormal function of cardiac potassium channels. *Cardiovascular research*, 116(9):1542–1556, 2020.

Lin Feng, Huibing Wang, Bo Jin, Haohao Li, Mingliang Xue, and Le Wang. Learning a distance metric by balancing kl-divergence for imbalanced datasets. *IEEE Transactions on Systems, Man, and Cybernetics: Systems*, 49(12):2384–2395, 2018.

João Pedro Ferreira, Javed Butler, Patrick Rossignol, Bertram Pitt, Stefan D Anker, Mikhail Kosiborod, Lars H Lund, George L Bakris, Matthew R Weir, and Faiez Zannad. Abnormalities of potassium in heart failure: Jacc state-of-the-art review. *Journal of the American College of Cardiology*, 75(22):2836–2850, 2020.

Conner D Galloway, Alexander V Valys, Jacqueline B Shreibati, Daniel L Treiman, Frank L Petterson, Vivek P Gundotra, David E Albert, Zachi I Attia, Rickey E Carter, Samuel J Asirvatham, et al. Development and validation of a deep-learning model to screen for hyperkalemia from the electrocardiogram. *JAMA cardiology*, 4(5):428–436, 2019.

Yu Gong, Greg Mori, and Fred Tung. RankSim: Ranking similarity regularization for deep imbalanced regression. In Kamalika Chaudhuri, Stefanie Jegelka, Le Song, Csaba Szepesvari, Gang Niu, and Sivan Sabato (eds.), *Proceedings of the 39th International Conference on Machine Learning*, volume 162 of *Proceedings of Machine Learning Research*, pp. 7634–7649. PMLR, 17–23 Jul 2022.

David M Harmon, Chris K Heinrich, John J Dillon, Rickey E Carter, Kianoush B Kashani, Zachi I Attia, Paul A Friedman, and Jacob C Jentzer. Mortality risk stratification utilizing artificial intelligence electrocardiogram for hyperkalemia in cardiac intensive care unit patients. *JACC: Advances*, pp. 101169, 2024.

Shenda Hong, Yanbo Xu, Alind Khare, Satria Priambada, Kevin O. Maher, Alaa Aljiffry, Jimeng Sun, and Alexey Tumanov. HOLMES: health online model ensemble serving for deep learning models in intensive care units. In Rajesh Gupta, Yan Liu, Jiliang Tang, and B. Aditya Prakash (eds.), *KDD '20: The 26th ACM SIGKDD Conference on Knowledge Discovery and Data Mining, Virtual Event, CA, USA, August 23-27, 2020*, pp. 1614–1624. ACM, 2020. doi: 10.1145/3394486.3403212.

Alistair Johnson, Lucas Bulgarelli, Tom Pollard, Steven Horng, Leo Anthony Celi, and Roger Mark. Mimic-iv. *PhysioNet. Available online at: https://physionet. org/content/mimiciv/1.0/(accessed August 23, 2021)*, pp. 49–55, 2020.

Mahsa Keramati, Lili Meng, and R. David Evans. Conr: Contrastive regularizer for deep imbalanced regression. In *The Twelfth International Conference on Learning Representations, ICLR 2024, Vienna, Austria, May 7-11, 2024*. OpenReview.net, 2024.

Michael J Kim, Christina Valerio, and Glynnis K Knobloch. Potassium disorders: hypokalemia and hyperkalemia. *American Family Physician*, 107(1):59–70A, 2023.

Gary King and Langche Zeng. Logistic regression in rare events data. *Political analysis*, 9(2): 137–163, 2001.

T Lin. Focal loss for dense object detection. *arXiv preprint arXiv:1708.02002*, 2017.

Ziwei Liu, Zhongqi Miao, Xiaohang Zhan, Jiayun Wang, Boqing Gong, and Stella X Yu. Large-scale long-tailed recognition in an open world. In *Proceedings of the IEEE/CVF conference on computer vision and pattern recognition*, pp. 2537–2546, 2019.

Stylianos Moschoglou, Athanasios Papaioannou, Christos Sagonas, Jiankang Deng, Irene Kotsia, and Stefanos Zafeiriou. Agedb: the first manually collected, in-the-wild age database. In *Proceedings of the IEEE Conference on Computer Vision and Pattern Recognition Workshop*, volume 2, pp. 5, 2017.

Emanuel Parzen. On estimation of a probability density function and mode. *The annals of mathematical statistics*, 33(3):1065–1076, 1962.

Jiawei Ren, Mingyuan Zhang, Cunjun Yu, and Ziwei Liu. Balanced mse for imbalanced visual regression. In *Proceedings of the IEEE/CVF Conference on Computer Vision and Pattern Recognition*, pp. 7926–7935, 2022.

Rasmus Rothe, Radu Timofte, and Luc Van Gool. Deep expectation of real and apparent age from a single image without facial landmarks. *International Journal of Computer Vision*, 126(2-4): 144–157, 2018.

Shiori Sagawa, Pang Wei Koh, Tatsunori B Hashimoto, and Percy Liang. Distributionally robust neural networks for group shifts: On the importance of regularization for worst-case generalization. *arXiv preprint arXiv:1911.08731*, 2019.

Chris Seiffert, Taghi M Khoshgoftaar, Jason Van Hulse, and Amri Napolitano. Rusboost: A hybrid approach to alleviating class imbalance. *IEEE transactions on systems, man, and cybernetics-part A: systems and humans*, 40(1):185–197, 2009.

Michael Steininger, Konstantin Kobs, Padraig Davidson, Anna Krause, and Andreas Hotho. Density-based weighting for imbalanced regression. *Machine Learning*, 110:2187–2211, 2021.

Junjiao Tian, Yen-Cheng Liu, Nathaniel Glaser, Yen-Chang Hsu, and Zsolt Kira. Posterior recalibration for imbalanced datasets. *Advances in neural information processing systems*, 33: 8101–8113, 2020.

Luís Torgo, Rita P Ribeiro, Bernhard Pfahringer, and Paula Branco. Smote for regression. In *Portuguese conference on artificial intelligence*, pp. 378–389. Springer, 2013.

Ziyan Wang and Hao Wang. Variational imbalanced regression: Fair uncertainty quantification via probabilistic smoothing. *Advances in Neural Information Processing Systems*, 36, 2024.

Yuzhe Yang, Kaiwen Zha, Yingcong Chen, Hao Wang, and Dina Katabi. Delving into deep imbalanced regression. In Marina Meila and Tong Zhang (eds.), *Proceedings of the 38th International Conference on Machine Learning*, volume 139 of *Proceedings of Machine Learning Research*, pp. 11842–11851. PMLR, 18–24 Jul 2021.

Ming Zheng, Tong Li, Rui Zhu, Yahui Tang, Mingjing Tang, Leilei Lin, and Zifei Ma. Conditional wasserstein generative adversarial network-gradient penalty-based approach to alleviating imbalanced data classification. *Information Sciences*, 512:1009–1023, 2020.

A APPENDIX

A.1 BASELINES

To ensure a fair comparison, we followed the experimental setup of Yang et al. (2021) on the IMDB-WIKI-DIR and AgeDB-DIR datasets, i.e., using ResNet-50 as the network architecture and training for 90 epochs. For the ECG-Ka-DIR dataset, we employed the ResNet variant Net1D Hong et al. (2020) as the network architecture. Given that previous work Yang et al. (2021); Ren et al. (2022); Gong et al. (2022); Keramati et al. (2024) has demonstrated superior performance over loss reweighting and regressor re-training (RRT) in deep imbalanced regression tasks, we do not include these methods as baselines in this paper. Instead, we focused on widely recognized approaches in the field: LDS, FDS Yang et al. (2021), Ranksim Gong et al. (2022), ConR Keramati et al. (2024), and Balanced MSE Ren et al. (2022). LDS and FDS encourage local similarities in label and feature space, while Ranksim and ConR leverage contrastive learning to translate label similarities into the feature space. Balanced MSE, based on label distribution priors, restores a balanced distribution from an imbalanced dataset. Our experimental findings indicate that not only does our method achieve SOTA performance in few-shot regions, but it also enhances existing methods, offering a complementary strategy to boost their efficacy.

A.2 IMPLEMENTATION DETAILS

We trained all models on the IMDB-WIKI-DIR and AgeDB-DIR datasets using a single NVIDIA GeForce RTX 3090 GPU and on the ECG-Ka-DIR dataset using a single NVIDIA GeForce RTX 4090 GPU. To ensure a fair comparison, we followed the training, validation, and test set divisions from Yang et al. (2021) for the IMDB-WIKI-DIR and AgeDB datasets. During training with Dist Loss, we used the same strategy as Balanced MSE, fine-tuning the linear layer based on pre-trained model (vanilla model) parameters. This approach integrates our method with existing methods, using their model parameters as the starting point for fine-tuning. Additionally, we used probability-based inversely weighted MSE to measure sequence difference in Dist Loss for all datasets, setting the distribution loss component weight to 1.

A.2.1 IMDB-WIKI-DIR

On the IMDB-WIKI-DIR dataset, we selected ResNet-50 as the network architecture. During training, the training epochs were set to 90, with an initial learning rate of 0.001, which was reduced to 1/10 of its value at the 60th and 80th epochs. We employed the Adam optimizer with a momentum of 0.9 and a weight decay of 0.0001. For our method and Balanced MSE, we used a batch size of 512. For the other baselines, we followed the experimental setups from their original papers. It should be noted that the original training epochs for Ranksim and ConR in their respective papers were 120, which we adjusted to 90 in our experiments to ensure a fair comparison.

A.2.2 AGEDB-DIR

On the AgeDB dataset, we employed ResNet-50 architecture for our model. The training consisted of 90 epochs with an initial learning rate of 0.001, which was reduced to 1/10 of its original value at the 60th and 80th epochs. We utilized the Adam optimizer with a momentum of 0.9 and a weight decay of 0.0001. For our method and Balanced MSE, we used a batch size of 512. For the other baselines, we followed the experimental configurations outlined in their respective original papers. To ensure a fair comparison, we also set the training epochs for Ranksim and ConR to 90.

A.2.3 ECG-KA-DIR

On the ECG-Ka-DIR dataset, we utilized the ResNet variant, Net1D Hong et al. (2020), as our network architecture. The training was set for 10 epochs with an initial learning rate of 0.001, which was reduced to 1/10 of its initial value at the 5th and 8th epochs. We employed the Adam optimizer with a momentum of 0.9 and a weight decay of 0.00001. A batch size of 512 was used for all methods. Additionally, for ConR, we constructed positive and negative sample pairs by adding Gaussian noise.

Table 6: Comprehensive results on the IMDB-WIKI-DIR dataset are presented. The table highlights the best results in each section using bold font. Additionally, the best result in each column is indicated in bold and red.

	MAE				GM			
	All	Many	Median	Few	All	Many	Median	Few
Vanilla	8.143	**7.260**	15.758	26.930	4.642	**4.211**	11.522	21.254
+ **Dist Loss**	**8.028**	7.461	**12.614**	**22.516**	**4.593**	4.335	**7.686**	**13.752**
+ LDS	8.036	**7.445**	12.869	22.753	**4.570**	**4.322**	7.528	**12.803**
+ **Dist Loss**	**8.017**	7.479	**12.304**	**22.331**	4.593	4.369	**7.078**	13.021
+ FDS	**7.954**	**7.272**	13.523	24.908	**4.499**	**4.192**	8.633	**14.361**
+ **Dist Loss**	8.712	8.163	**12.979**	**24.112**	5.222	4.995	**7.575**	14.929
+ Ranksim	7.764	**6.956**	14.606	25.999	**4.371**	**3.996**	9.964	19.690
+ Dist Loss	**7.721**	7.129	**12.401**	**23.772**	4.422	4.183	**7.091**	**15.422**
+ ConR	**7.842**	**7.033**	14.772	25.408	**4.329**	**3.951**	10.250	17.022
+ Dist Loss	7.957	7.355	**12.906**	**22.700**	4.529	4.244	**8.131**	**14.713**
Balanced MSE	**8.033**	**7.441**	12.768	23.542	4.716	4.450	8.035	**12.603**
+ Dist Loss	8.075	7.511	**12.625**	**22.597**	**4.616**	**4.354**	**7.754**	14.238

Table 7: Comprehensive results on the AgeDB-DIR dataset are presented. The table highlights the best results in each section using bold font. Additionally, the best result in each column is indicated in bold and red.

	MAE				GM			
	All	Many	Median	Few	All	Many	Median	Few
Vanilla	**7.506**	**6.558**	8.794	12.894	4.798	**4.176**	5.957	9.789
+ Dist Loss	7.637	7.574	**7.315**	**9.122**	**4.756**	4.745	**4.563**	**5.453**
+ LDS	**7.783**	**7.070**	8.957	11.279	5.088	**4.599**	6.142	7.846
+ Dist Loss	7.810	7.341	**8.464**	**10.437**	**5.043**	4.752	**5.474**	**7.051**
+ FDS	7.818	**7.103**	9.051	11.161	4.961	**4.487**	6.064	7.361
+ Dist Loss	**7.799**	7.351	**8.374**	**10.444**	**4.863**	4.615	**5.181**	**6.696**
+ Ranksim	7.272	**6.363**	8.458	12.569	**4.617**	**3.939**	6.120	9.495
+ Dist Loss	**7.234**	6.506	**7.960**	**12.102**	4.629	4.097	**5.637**	**8.515**
+ ConR	**7.322**	**6.429**	8.456	12.623	**4.646**	**4.052**	5.890	**8.787**
+ Dist Loss	7.383	6.572	**8.373**	**12.303**	4.657	4.112	**5.591**	9.123
Balanced MSE	7.663	**7.540**	7.353	9.613	**4.658**	**4.558**	4.511	6.248
+ Dist Loss	**7.633**	7.578	**7.288**	**9.110**	4.718	4.698	**4.505**	**5.585**

Table 8: Comprehensive results on the ECG-Ka-DIR dataset are presented. The table highlights the best results in each section using bold font. Additionally, the best result in each column is indicated in bold and red.

	MAE				GM			
	All	Many	Median	Few	All	Many	Median	Few
Vanilla	1.235	**0.274**	0.685	1.771	0.835	**0.193**	0.622	1.578
+ Dist Loss	**1.044**	0.606	**0.674**	**1.329**	**0.692**	0.403	**0.445**	**0.978**
+ LDS	1.092	**0.368**	**0.638**	1.510	0.708	**0.236**	0.500	1.190
+ Dist Loss	**1.031**	0.557	0.671	**1.325**	**0.671**	0.363	**0.455**	**0.957**
+ FDS	1.223	**0.317**	**0.681**	1.737	0.828	**0.201**	0.588	1.529
+ Dist Loss	**1.095**	0.557	0.688	**1.428**	**0.744**	0.375	**0.490**	**1.099**
+ Ranksim	1.249	**0.275**	0.696	1.791	0.841	**0.190**	0.629	1.600
+ Dist Loss	**1.040**	0.587	**0.683**	**1.325**	**0.692**	0.381	**0.487**	**0.970**
+ ConR	1.227	**0.277**	0.690	1.756	0.824	**0.189**	0.620	1.556
+ Dist Loss	**1.045**	0.581	**0.684**	**11.336**	**0.696**	0.376	**0.480**	**0.987**
Balanced MSE	1.106	0.606	0.727	1.417	0.722	0.383	0.475	1.046
+ Dist Loss	**1.046**	**0.553**	**0.658**	**1.357**	**0.685**	**0.358**	**0.454**	**0.996**

Table 9: Ablation study examining the impact of batch size on model performance across the IMDB-WIKI-DIR, AgeDB-DIR, and ECG-Ka-DIR datasets.

Dataset	Batch size	MAE				GM			
		All	Many	Median	Few	All	Many	Median	Few
IMDB-WIKI-DIR	256	8.072	7.514	12.591	22.323	4.603	4.340	7.808	13.787
	512	8.028	7.461	12.614	22.516	4.593	4.335	7.686	13.752
	768	7.989	7.413	12.663	22.550	4.572	4.308	7.763	14.288
AgeDB-DIR	256	8.072	7.514	12.591	22.323	4.603	4.340	7.808	13.787
	512	8.028	7.461	12.614	22.516	4.593	4.335	7.686	13.752
	1024	7.989	7.413	12.663	22.550	4.572	4.308	7.763	14.288
ECG-Ka-DIR	256	8.072	7.514	12.591	22.323	4.603	4.340	7.808	13.787
	512	8.028	7.461	12.614	22.516	4.593	4.335	7.686	13.752
	1024	7.989	7.413	12.663	22.550	4.572	4.308	7.763	14.288

A.3 Comprehensive experimental results

Tables 6, 7, and 8 present a comprehensive overview of our experimental results on the IMDB-WIKI-DIR, AgeDB-DIR, and ECG-Ka-DIR datasets. The results indicate that our method achieves improvements in model performance on median-shot and few-shot regions without compromising overall error rates. This further demonstrates the effectiveness of our method in sparse data regions.

A.4 Ablations and analysis

A.4.1 Different batch sizes for distribution distance approximation

Table 9 illustrates the impact of varying batch sizes on the final performance across three datasets: IMDB-WIKI-DIR, AgeDB-DIR, and ECG-Ka-DIR. The results indicate that there is no significant difference in performance among different batch sizes. This observation suggests that the generation of pseudo-labels primarily requires an approximation of the distribution information, rather than the precise accuracy of every individual label value.

A.4.2 Different loss functions for sequence difference measurement.

Tables 10, 11, and 12 present the comprehensive results of using different loss functions on IMDB-WIKI-DIR, AgeDB-DIR, and ECG-Ka-DIR, respectively. It is evident that existing methods, when augmented with Dist Loss, demonstrate superior performance on samples within few-shot regions.

A.4.3 Performance of Dist Loss across different imbalanced ratios

We validated the effectiveness of Dist Loss by varying the imbalance ratios of the ECG-Ka-DIR dataset. The data distribution diagrams are shown in Figure 4, and the corresponding results in the few-shot regions are presented in Table 13. Across eight datasets with different imbalance ratios, our method achieved the best performance in six cases and the second-best performance in the remaining two. These results collectively demonstrate the robustness of our approach across varying levels of data imbalance.

A.5 Performance of Dist Loss on the GM Metric

We observed that on the IMDB-WIKI-DIR dataset, the performance of Dist Loss in the few-shot region, as measured by the GM metric, is inferior to that of Balanced MSE. To provide a more intuitive analysis of this phenomenon, we plotted the **sorted error distribution curves** for both Dist Loss and Balanced MSE in the few-shot region, as shown in Figure 5. Specifically, for each method, the error values were first sorted in ascending order. The x-axis represents the rank of these sorted errors, while the y-axis denotes the corresponding error magnitudes. This visualization facilitates a direct comparison of the error distributions between the two methods.

Table 10: An ablation study on loss functions on the IMDB-WIKI-DIR dataset. L_1 represents MAE Loss, L_2 represents MSE Loss, $INV-$ denotes the probability-based inversely weighted version of these loss functions. Results on the few-shot region are reported.

	MAE				GM			
	All	Many	Median	Few	All	Many	Median	Few
Vanilla	8.143	7.260	15.758	26.930	4.642	4.211	11.522	21.254
+ Dist Loss ($INV - L_1$)	7.807	7.210	12.608	23.334	4.458	4.189	7.717	15.437
+ Dist Loss ($INV - L_2$)	8.028	7.461	12.614	22.516	4.593	4.335	7.686	13.752
+ LDS	8.036	7.445	12.869	22.753	4.570	4.322	7.528	12.803
+ Dist Loss ($INV - L_1$)	8.054	7.545	12.030	22.178	4.678	4.486	6.717	11.334
+ Dist Loss ($INV - L_2$)	8.017	7.479	12.304	22.331	4.593	4.369	7.078	13.021
+ FDS	7.954	7.272	13.523	24.908	4.499	4.192	8.633	14.361
+ Dist Loss ($INV - L_1$)	7.986	7.413	12.486	23.692	4.530	4.315	6.793	14.399
+ Dist Loss ($INV - L_2$)	8.712	8.163	12.979	24.112	5.222	4.995	7.575	14.929
+ Ranksim	7.764	6.956	14.606	25.999	4.371	3.996	9.964	19.690
+ Dist Loss ($INV - L_1$)	7.501	6.888	12.372	23.894	4.150	3.910	7.035	16.036
+ Dist Loss ($INV - L_2$)	7.721	7.129	12.401	23.772	4.422	4.183	7.091	15.422
+ ConR	7.842	7.033	14.772	25.408	4.329	3.951	10.25	17.022
+ Dist Loss ($INV - L_1$)	7.538	6.924	12.499	23.281	4.169	3.893	7.643	15.586
+ Dist Loss ($INV - L_2$)	7.957	7.355	12.906	22.700	4.529	4.244	8.131	14.713
+ Balanced MSE	8.033	7.441	12.768	23.542	4.716	4.450	8.035	12.603
+ Dist Loss ($INV - L_1$)	7.788	7.175	12.732	23.539	4.460	4.182	7.900	15.000
+ Dist Loss ($INV - L_2$)	8.075	7.511	12.625	22.597	4.616	4.354	7.754	14.238

Table 11: An ablation study on loss functions on the AgeDB-DIR dataset. L_1 represents MAE Loss, L_2 represents MSE Loss, $INV-$ denotes the probability-based inversely weighted version of these loss functions. Results on the few-shot region are reported.

	MAE				GM			
	All	Many	Median	Few	All	Many	Median	Few
Vanilla	7.506	6.558	8.794	12.894	4.798	4.176	5.957	9.789
+ Dist Loss ($INV - L_1$)	7.552	7.282	7.660	9.802	4.700	4.528	4.800	6.298
+ Dist Loss ($INV - L_2$)	7.637	7.574	7.315	9.122	4.756	4.745	4.563	5.453
+ LDS	7.783	7.070	8.957	11.279	5.088	4.599	6.142	7.846
+ Dist Loss ($INV - L_1$)	7.885	7.635	8.020	9.872	5.082	4.964	5.151	6.109
+ Dist Loss ($INV - L_2$)	7.810	7.341	8.464	10.437	5.043	4.752	5.474	7.051
+ FDS	7.818	7.103	9.051	11.161	4.961	4.487	6.064	7.361
+ Dist Loss ($INV - L_1$)	7.911	7.665	8.010	9.969	5.010	4.933	4.941	6.026
+ Dist Loss ($INV - L_2$)	7.799	7.351	8.374	10.444	4.863	4.615	5.181	6.696
+ Ranksim	7.272	6.363	8.458	12.569	4.617	3.939	6.120	9.495
+ Dist Loss ($INV - L_1$)	7.239	6.605	7.727	11.877	4.635	4.194	5.311	8.164
+ Dist Loss ($INV - L_2$)	7.234	6.506	7.960	12.102	4.629	4.097	5.637	8.515
+ ConR	7.322	6.429	8.456	12.623	4.646	4.052	5.890	8.787
+ Dist Loss ($INV - L_1$)	7.398	6.683	8.194	11.948	4.709	4.208	5.560	8.605
+ Dist Loss ($INV - L_2$)	7.383	6.572	8.373	12.303	4.657	4.112	5.591	9.123
+ Balanced MSE	7.663	7.540	7.353	9.613	4.658	4.558	4.511	6.248
+ Dist Loss ($INV - L_1$)	7.537	7.300	7.540	9.762	4.751	4.623	4.737	6.198
+ Dist Loss ($INV - L_2$)	7.633	7.578	7.288	9.110	4.718	4.698	4.505	5.585

Table 12: An ablation study on loss functions on the ECG-Ka-DIR dataset. L_1 represents MAE Loss, L_2 represents MSE Loss, $INV-$ denotes the probability-based inversely weighted version of these loss functions. Results on the few-shot region are reported.

	MAE				GM			
	All	Many	Median	Few	All	Many	Median	Few
Vanilla	1.235	0.274	0.685	1.771	0.835	0.193	0.622	1.578
+ Dist Loss ($INV - L_1$)	1.088	0.458	0.648	1.467	0.680	0.300	0.463	1.044
+ Dist Loss ($INV - L_2$)	1.044	0.606	0.674	1.329	0.692	0.403	0.445	0.978
+ LDS	1.092	0.368	0.638	1.510	0.708	0.236	0.500	1.190
+ Dist Loss ($INV - L_1$)	1.059	0.463	0.655	1.413	0.647	0.291	0.445	0.984
+ Dist Loss ($INV - L_2$)	1.031	0.557	0.671	1.325	0.671	0.363	0.455	0.957
+ FDS	1.223	0.317	0.681	1.737	0.828	0.201	0.588	1.529
+ Dist Loss ($INV - L_1$)	1.133	0.497	0.692	1.515	0.725	0.324	0.477	1.122
+ Dist Loss ($INV - L_2$)	1.095	0.557	0.688	1.428	0.744	0.375	0.490	1.099
+ Ranksim	1.249	0.275	0.696	1.791	0.818	0.215	0.566	1.510
+ Dist Loss ($INV - L_1$)	1.139	0.394	0.649	1.577	0.712	0.317	0.472	1.099
+ Dist Loss ($INV - L_2$)	1.040	0.587	0.683	1.325	0.723	0.400	0.479	1.031
+ ConR	1.227	0.277	0.69	1.756	0.841	0.190	0.629	1.600
+ Dist Loss ($INV - L_1$)	1.085	0.484	0.651	1.452	0.780	0.272	0.503	1.330
+ Dist Loss ($INV - L_2$)	1.045	0.581	0.684	1.336	0.692	0.381	0.486	0.970
+ Balanced MSE	1.106	0.606	0.727	1.417	0.824	0.189	0.620	1.556
+ Dist Loss ($INV - L_1$)	1.092	0.457	0.65	1.474	0.678	0.307	0.443	1.044
+ Dist Loss ($INV - L_2$)	1.046	0.553	0.658	1.357	0.696	0.376	0.480	0.987

Table 13: Performance of Dist Loss in the few-shot regions across eight datasets derived from the ECG-Ka-DIR dataset with varying imbalance ratios, with the best results highlighted in bold.

	MAE							
Methods	Dataset 0	Dataset 1	Dataset 2	Dataset 3	Dataset 4	Dataset 5	Dataset 6	Dataset 7
Vanilla	2.701	2.676	2.658	1.979	2.679	2.647	2.624	1.888
LDS	2.684	2.703	2.642	1.962	2.672	2.507	2.644	1.901
FDS	**1.865**	2.368	2.191	**1.790**	2.223	2.625	1.908	1.665
Ranksim	2.470	2.327	2.273	1.831	2.314	2.192	2.258	1.725
ConR	2.461	2.343	2.308	1.828	2.193	2.274	2.255	1.742
Balanced MSE	1.997	1.984	1.981	1.831	1.906	1.863	1.815	1.708
Dist Loss	1.955	**1.873**	**1.963**	1.822	**1.852**	**1.803**	**1.730**	**1.638**

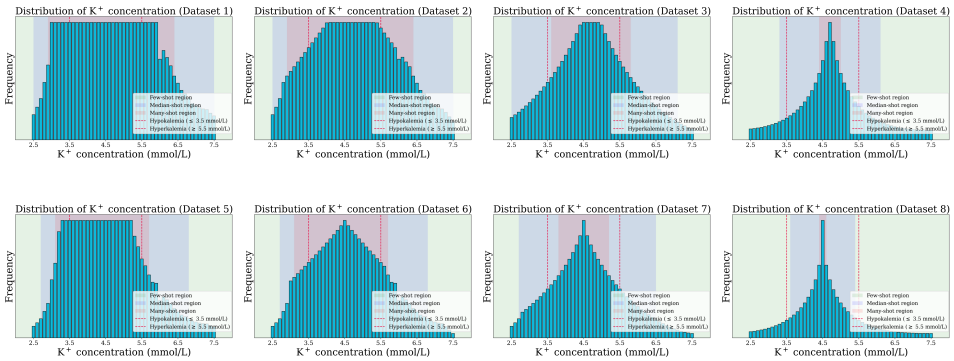

Figure 4: Data distribution diagrams for the eight datasets derived from the ECG-Ka-DIR dataset with varying imbalance ratios.

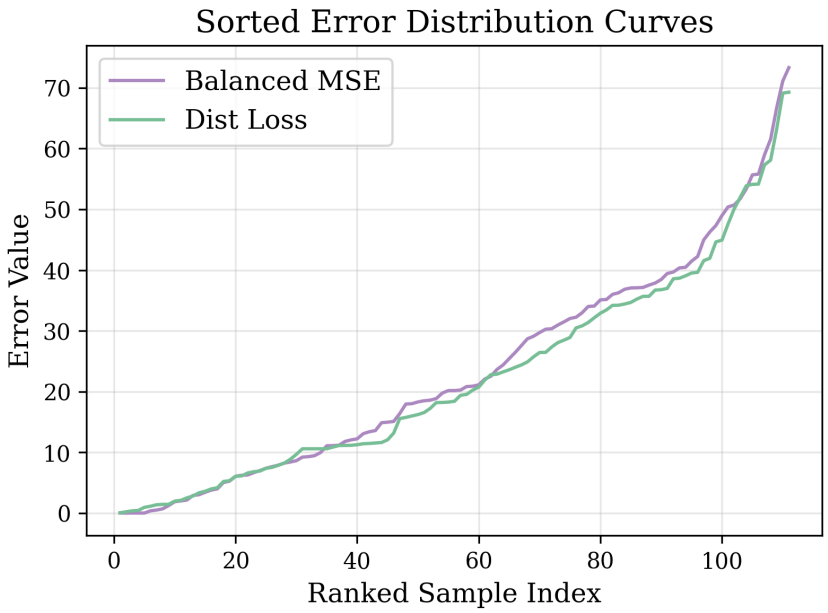

Figure 5: Sorted error distribution curves for Dist Loss and Balanced MSE in the few-shot region on the IMDB-WIKI-DIR dataset.

From the plot, it is evident that Dist Loss generally exhibits superior performance compared to Balanced MSE, as indicated by its curve lying below or aligning with the curve for Balanced MSE. However, a localized discrepancy is observed around the x-axis values of approximately 5 and 30, where the errors of Dist Loss slightly exceed those of Balanced MSE. We hypothesize that this localized discrepancy may contribute to the overall inferior performance of Dist Loss in terms of the GM metric, owing to the **cumulative multiplicative effect** intrinsic to its calculation. Unlike MAE, which averages error values, the GM metric calculates the geometric mean by multiplying error values together. This process significantly amplifies the impact of small but frequent errors. For example, consider two error distributions: $(40, 10.1, 10.1, 10.1, 10.1, 10.1)$ and $(42, 10, 10, 10, 10, 10)$. While the former achieves a lower MAE than the latter, its GM metric value is higher due to the cumulative effect, as $40 \times 1.01^5 > 42 \times 10^5$. This example underscores how the GM metric can magnify the influence of small deviations when they occur frequently.

In conclusion, the sorted error distribution curves demonstrate that Dist Loss consistently achieves better or comparable performance relative to Balanced MSE, except for minor localized discrepancies. These results suggest that the unique characteristics of the GM metric are the primary factors contributing to the observed differences in performance between the two methods.